PHYSICAL REVIEW B VOLUME 50, NUMBER 15 15 OCTOBER 1994-I

Atomic imaging by x-ray-fluorescence holography and electron-emission holography: A comparative theoretical study

P. M. Len, S. Thevuthasan,* and C. S. Fadley†
Department of Physics, University of California at Davis, Davis, California 95616

A. P. Kaduwela and M. A. Van Hove
Materials Sciences Division, Lawrence Berkeley Laboratory, Berkeley, California 94720
(Received 5 August 1994)

We consider from a theoretical viewpoint the direct imaging of atoms at and near the surfaces of solids by both x-ray-fluorescence holography (XFH) and electron-emission holography (EEH). The more ideal nature of x-ray scattering makes XFH images superior to those in single-energy EEH. The overlap of real and twin features for pairs of atoms at $\pm\mathbf{a}$ can cause their XFH or EEH atomic images to cancel for certain combinations of wave vector and $|\mathbf{a}|$. The relative merits of XFH and EEH for structure studies are considered.

In 1985 Szöke pointed out that the interference patterns produced in the emission of photoelectrons or characteristic x rays from localized core levels could be thought of as holograms.[1] The unscattered electron or x-ray component from an emitting atom that reaches a distant detector is in this case considered to be the holographic reference wave, while the components that scatter from neighboring atoms before reaching the detector are the object waves. The interference pattern created by the reference and object waves is then an electron-emission hologram (EEH), or an x-ray-fluorescence hologram (XFH). A simple method for producing atomic images from such holograms makes use of the Helmholtz-Kirchhoff theorem, as discussed by Barton:[2(a)]

$$U(\mathbf{r}) \propto \int\int_S \chi(\mathbf{k}) \exp(-i\mathbf{k}\cdot\mathbf{r}) d\sigma_k , \tag{1}$$

where $|U(\mathbf{r})| \equiv U^0(\mathbf{r})$ is the image of the atomic scatterers as evaluated at position $\mathbf{r}$, $\chi(\mathbf{k})$ is the normalized interference pattern, $\mathbf{k}$ is the emission wave vector, and the integral is over the surface of constant $k=|\mathbf{k}|$ for which intensities have been measured. Applications of this procedure to both experimental EEH data and theoretical simulations of it have been discussed in several prior papers,[2–6] where it has been shown to be capable of probing the *short-range* atomic structure around a given emitter type. Several categories of image distortions and aberrations have been identified, and possible methods for correcting them have been discussed.[2–6] One correction method suggested by Barton[2(b)] is the phased summation of integrals such as that in Eq. (1), obtained for several different energies (i.e., k values) to yield a new image $U^1(\mathbf{r})$ as

$$U^1(\mathbf{r}) = \left| \sum_{j=1}^{n} U_j(\mathbf{r}) \exp(ik_j r) \Delta k \right| . \tag{2}$$

The only previous attempt to assess the application of the holographic methodology of Eq. (1) to XFH was a theoretical study by Tegze and Faigel.[7] This work is also related to prior suggestions of using the interference maxima in Kossel lines from specimens with long-range order to solve the phase problem in x-ray-diffraction structure determinations.[8,9] The use of Kossel lines requires *long-range* order in the specimen as manifested by sharp Bragg-like interference effects in outgoing fluorescence x rays, while in XFH it is desired to probe short-range order associated with lower-frequency Fourier components in $\chi(\mathbf{k})$. Coupled with the fact that *all* scattering from atoms further away from the emitter will be associated with higher-frequency components in $\chi(\mathbf{k})$, this has led to the suggestion of Fourier-filtering emission patterns so as to focus on near-neighbor atomic positions only.[7] In this paper, we have carried out a comparison of model calculations for EEH and XFH images in the same short-range-order picture, using the well-known single-scattering cluster model[6] to generate the initial full 2π solid-angle holograms above a surface for both cases; unless otherwise noted, intensities were calculated on a $1°\times1°$ grid in polar and azimuthal angles. As a part of this paper, we also have verified that Fourier-filtering $\chi(\mathbf{k})$ holograms effectively eliminate the effects of scattering from atoms at large distances from the emitter, even with the weak inelastic attenuation appropriate to x rays.

EEH and XFH holograms were calculated for emission from a planar cluster of 49 Mo atoms simulating a domain of short-range order on the Mo(001) surface and consisting of a square array with lattice constant 3.15 Å [Fig. 1(a)]. To permit direct comparison of image quality and resolution, the electron and x-ray emission processes have both been assumed to generate reference waves with s character outgoing from the emitter, and have also been chosen to have the same de Broglie wavelength of $\lambda=0.62$ Å (wave vector of 10.1 $Å^{-1}$), corresponding to electrons at 391 eV and x rays at 20 keV (very near the Mo $K\beta$ energy of 19.6 keV). Exponential attenuation due to inelastic scattering of electrons or absorption of x rays for propagation within the cluster has also been incorporated, with decay lengths of 7.6 Å for electrons and 5×10^5 Å for x rays. Attenuation is thus taken to be isotropic in space, an assumption that is expected to be fully valid in this short-range-order limit, as verified, for example, in prior studies of photoelectron and low-energy electron-diffraction studies,[6,10(a)] and of the absorption and transmission of x rays in specimens without long-range order.[10(b)]

Holographic images derived from these calculated holograms using Eq. (1) are shown in Figs. 1(b) and 1(c). Also,

0163-1829/94/50(15)/11275(4)/$06.00

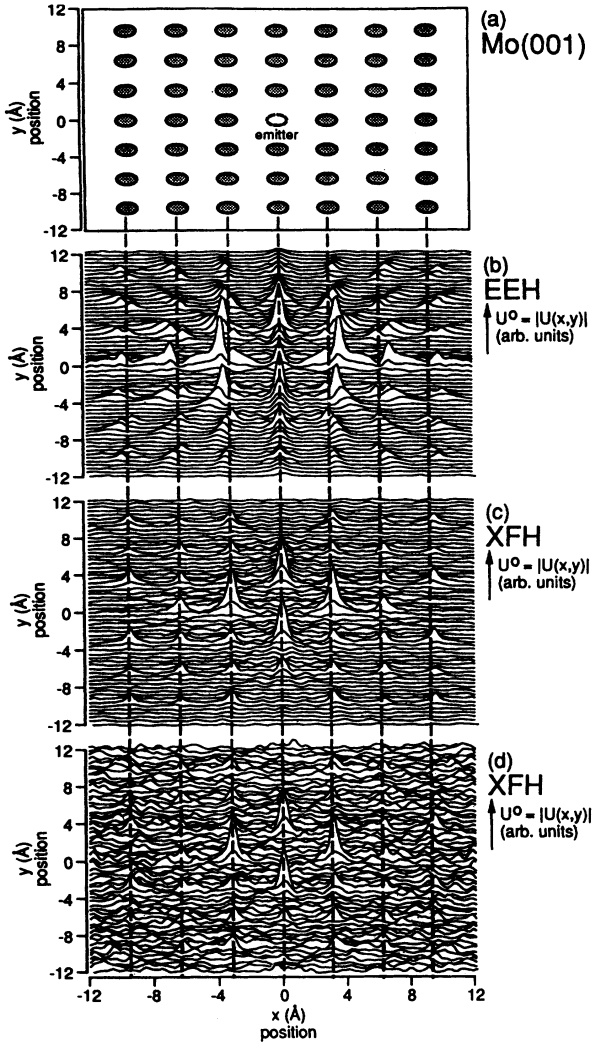

FIG. 1. (a) 49-atom Mo(001) cluster in the xy plane at $z=0.0$ Å. (b) Image of the cluster in (a) as derived from the calculated electron-emission hologram (EEH) at 391 eV. (c) Image of the same cluster as derived from the calculated x-ray-fluorescence hologram (XFH) at 20.0 keV. Both electrons and x rays have a wavelength of 0.620 Å. (d) Image of the same cluster as derived from a simulated experimental XFH with statistical noise appropriate to 10^9 counts per direction.

shown in Fig. 1(d) is an image derived from a simulated experimental XFH hologram calculated on a more coarse $3°\times3°$ grid and including random statistical noise characteristic of a total average count of 10^9 in each direction; counting to less than this value (e.g., 10^8) was found to lead to image deterioration. As expected from prior studies,[2–6] the image peaks in EEH [Fig. 1(b)] are within 0.5 Å of their true atomic positions; however, the XFH image peaks [Figs. 1(c) and 1(d)] are much more accurately located to within 0.1 Å or less. Also, the XFH images do not have the characteristic elongations and satellite features that are present in those of Fig. 1(b) and other single-energy EEH images obtained to date.[2–6]

This difference in image quality is expected in view of the much more ideal nature of x-ray scattering from atoms, which is illustrated quantitatively for Mo in Fig. 2. The scat-

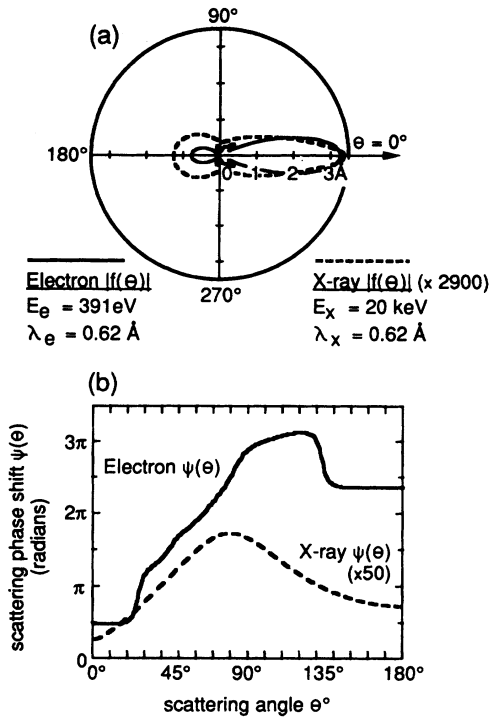

FIG. 2. Scattering factors $f(\Theta)=|f(\Theta)|\exp[i\psi(\Theta)]$ for electrons and x rays with the same wavelength of 0.620-Å scattering from Mo; Θ is the scattering angle. (a) Polar plots of the magnitude $|f(\Theta)|$ in Å for electrons and x rays. (b) Phase shifts $\psi(\Theta)$ (radians) as a function of scattering angle Θ (degrees).

tering factor for electrons was computed from muffin-tin partial-wave phase shifts using an accurate spherical-wave method;[6] that for x rays was calculated from standard tables of the quantity $f=f_0+\Delta f'+i\Delta f''$ as a function of scattering angle Θ and wavelength λ_x through $\sin\Theta/\lambda_x$ (Ref. 11) to yield both a magnitude $|f(\Theta)|$ and phase $\psi(\Theta)$. Figure 2(a) shows that both x-ray and electron scattering factors have maximum magnitudes in the forward direction, but x-ray scattering is much more isotropic and is for this case about 2900× lower in magnitude than that for electrons. Figure 2(b) shows that the x-ray-scattering phase shift is negligible when compared to that for electrons, with the latter also depending strongly on the scattering direction. The only disadvantage—but a significant one—of using x rays is therefore that the magnitude of the scattering factor will be about 10^3–10^4 times lower for a given wavelength, leading to similarly reduced fractional diffraction anisotropies in the normalized holograms ($\Delta I/I_{\max}\approx0.5$–$1.0$ for electrons and $\approx10^{-4}$ for x rays in the present calculations).

An additional important effect in the quantitative analysis of *all* EEH or XFH images is seen in our results: for certain choices of wavelength and atomic positions, the images of certain symmetry-related pairs of scattering atoms are strongly suppressed. An example of this effect can be seen in Fig. 1(c) by comparing the relative strengths of features due to different scatterers near the emitter: note the missing atomic images in XFH at $(x,y)=(0.0\text{ Å},\pm9.45\text{ Å})$ and $(\pm9.45\text{ Å},0.0\text{ Å})$. This image cancellation was qualitatively discussed by Tegze and Faigel[7] for XFH, and is due to the overlap of the complex-conjugate real and twin features in U^0 for atomic pairs located at $\pm\mathbf{a}$.

This image cancellation can be quantitatively understood in general for both EEH and XFH by applying the algorithm of Eq. (1) to a pair of scattering atoms situated at $\pm\mathbf{a}$ in the x-y surface plane (assumed to be perpendicular to the z axis of cylindrical symmetry of the hologram). We also assume that the two atoms are illuminated equally by the reference wave (as is the case with our previous assumption of s character). The reconstructed image at $\mathbf{r}$ of a *single* atomic scatterer located at $+\mathbf{a}$ can then be written in a single scattering picture as[6]

$$U(\mathbf{r})\propto\int\int_S\{f^*(\Theta_+)\exp(-ika)\exp[i\mathbf{k}\cdot(\mathbf{a}-\mathbf{r})] +f(\Theta_+)\exp(ika)\exp[i\mathbf{k}\cdot(-\mathbf{a}-\mathbf{r})]\}d\sigma_k, \quad (3)$$

where the f's are atomic scattering factors, and Θ_+ is the scattering angle between $+\mathbf{a}$ and $\mathbf{k}$. The first term contributes to the real image at $\mathbf{r}=+\mathbf{a}$, and the second term to the twin image at $\mathbf{r}=-\mathbf{a}$. As $|\mathbf{a}|$ varies for a given k, the image function $U(\mathbf{r})$ thus oscillates between being pure real and pure imaginary due to the phase factors $\exp(\pm ika)$ associated with path-length differences. For a *pair* of scattering atoms at $\pm\mathbf{a}$ [Fig. 3(a)], the atomic image at the special point $\mathbf{r}=+\mathbf{a}$ is thus the superposition of the actual image from the $+\mathbf{a}$ atom and the twin image from the $-\mathbf{a}$ atom:

$$U(\mathbf{r}=+\mathbf{a})\propto\exp(-ika)\int\int_S f^*(\Theta_+)d\sigma_k +\exp(ika)\int\int_S f(\Theta_-)d\sigma_k, \quad (4)$$

where Θ_- $(=\pi-\Theta_+)$ is the angle between $-\mathbf{a}$ and $\mathbf{k}$. For such a pair of equally illuminated scatterers in a plane perpendicular to the symmetry axis of the hologram, we further note that

$$\int\int_S f(\Theta_+)d\sigma_k=\int\int_S f(\Theta_-)d\sigma_k. \quad (5)$$

Then the image at $\mathbf{r}=+\mathbf{a}$ of the $\pm\mathbf{a}$ pair becomes

$$U(\mathbf{r}=+\mathbf{a})\propto\cos(ka)\int\int_S\mathrm{Re}[f(\Theta_+)]d\sigma_k -\sin(ka)\int\int_S\mathrm{Im}[f(\Theta_+)]d\sigma_k. \quad (6)$$

There can thus be values of ka such that the image at $\mathbf{r}=+\mathbf{a}$ disappears, with the general condition for image cancellation being

$$\tan(ka)=\int\int_S\mathrm{Re}[f(\Theta_+)]d\sigma_k\Big/\int\int_S\mathrm{Im}[f(\Theta_+)]d\sigma_k. \quad (7)$$

In the case of x-ray scattering, $\mathrm{Im}f(\Theta_\pm)\approx 0$, so the cancellation condition in Eq. (7) can be simplified to $ka=\pi(2m+1)/2$, with m equal to some nonzero integer. So when $|\mathbf{a}|=\lambda(2m+1)/4$, pairs of atoms at $\pm\mathbf{a}$ cannot be imaged. The missing atomic images in Figs. 1(c) and 1(d) are in fact found to correspond to the cancellation condition for $m=30$.

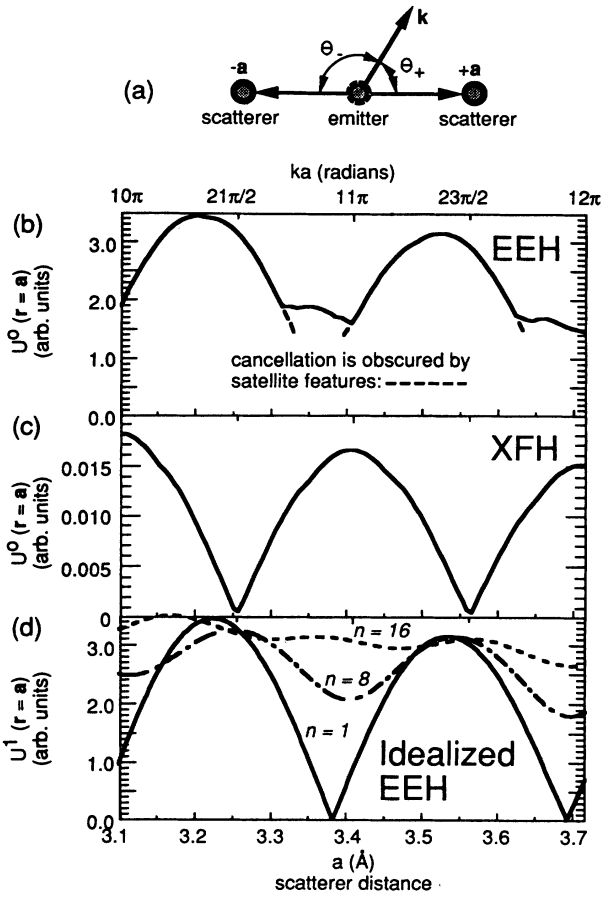

FIG. 3. (a) Three-atom Mo cluster, with a variable emitter-scatterer separation $|\mathbf{a}|$. Θ_+ is the scattering angle between $+\mathbf{a}$ and $\mathbf{k}$, and Θ_- is the scattering angle between $-\mathbf{a}$ and $\mathbf{k}$. Holographic reconstruction magnitudes $U^0(\mathbf{r}=\mathbf{a})$ and $U^1(\mathbf{r}=\mathbf{a})$ for the scatterer at $+\mathbf{a}$ as a function of $|\mathbf{a}|$ for (b) single-energy EEH; (c) single-energy XFH; (d) idealized phase-summed EEH using n different wave-number constructions.

Figure 3 shows the image magnitude $U^0=|U|$ at $\mathbf{r}=+\mathbf{a}$ as a function of $|\mathbf{a}|$ for the three-atom cluster in the top panel. The expected sinusoidal dependence of the XFH image intensities is apparent in Fig. 3(c), for which the minima can be well predicted from $ka=\pi(2m+1)/2$. For electrons [Fig. 3(b)], the same effects are clearly seen also, although the cancellation minima of the atomic peaks are masked by the broad satellite images that surround them [cf. Fig. 1(b)].

Such suppression of certain peaks could make the relative intensities in holographic images difficult to interpret for high-symmetry experimental geometries such as that considered here. However, this undesirable real-twin interference may be partially remedied by breaking the symmetry conditions leading to Eq. (5), for example, by using only a selected part of the full 2π hologram solid angle above the bulk surface,[4] or by orienting the exciting polarization vector in photoelectron holography so that the atoms at $\pm\mathbf{a}$ are inequivalent in their illumination by the outgoing reference wave. A more general solution is to remove twin images by using a phased summation of reconstructions at different k values,[2(b),5] as in Eq. (2). To illustrate how the latter would function, we insert Eq. (4) in Eq. (2) and find in the limit of

an integral over continuously distributed k values:

$$U^1(\mathbf{r}=+\mathbf{a}) \propto \left| \int_k \int \int_S f^*(\Theta_+) d\sigma_k dk \right| . \quad (8)$$

Here, image cancellation is seen to be eliminated, as the twin image term proportional to $f(\Theta_-)$ in Eq. (4) does not survive the integration on k. To assess the behavior of such images for the practical case of summations over a finite k range and finite n, we show in Fig. 3(d) a series of calculations. The solid curve represents the EEH image magnitude $U^0=|U|$ at $\mathbf{r}=+\mathbf{a}$ as a function of $|\mathbf{a}|$, as obtained from Eq. (6), which idealizes the cancellation of EEH atomic images, and thus does not include the presence of satellite features. Also shown are broken curves representing phased summations U^1 from Eq. (2) of various numbers n of different wave-number reconstructions, all with $k_{\text{initial}}=10.1$ Å^{-1}, and a numerical integration increment $\Delta k=0.3$ Å^{-1}. After phase summing just two wave-number reconstructions, there is no longer complete suppression of image peaks. Increasing the number of reconstructions in the sum gradually removes the modulation of the image intensity, and by 10–15 images, it is reduced to an acceptable level.

Note that while phased summing would also in principle remove the cancellation effect in XFH images (as well as other image aberrations due to twins and multiple scattering[2(b)]), it would not be experimentally feasible to carry out. The number and spacing of different wave-number reconstructions available would be severely limited by the characteristic fluorescence energies of the emitting atom. In Auger-electron holography, a similar limitation would apply. But in photoelectron holography,[3–6] back-scattered Kikuchi-electron holography,[12] or the holographic analysis of elastic diffuse low-energy electron diffraction,[13] simply varying photon energy or incident electron energy should permit such summations over a sufficient number of energies.

In conclusion, the weaker, more s-like scattering of x rays causes XFH reconstructions to yield significantly better atomic images than those of EEH reconstructions. At comparable wavelengths, XFH images should be approximately an order of magnitude more accurate than those of EEH, yielding atomic positions to within 0.1 Å or less, and they should be much less troubled by image distortions and satellites. The much greater attenuation lengths of x rays (5×10^5 Å compared to 7.6 Å for electrons in the Mo case considered here) would in general make XFH more of a bulk long-range-order probe, unless it is applied to atoms in a mosaic crystal or a thin adsorbed or epitaxial overlayer with limited domain sizes, and/or studied in a grazing emergence condition. Although the much weaker scattering of x rays will reduce relative effects by 10^3–10^4 times, it is nonetheless of interest to explore XFH experimentally in the future, combining high-brightness synchrotron radiation (SR) for excitation with some form of multichannel detection to shorten data acquisition times. The 10^9 statistics used in arriving at Fig. 1(d) also make it appear that such data are feasible to obtain in a reasonable time of several days, with parallel detection and an x-ray wiggler or undulator for excitation. For example, it should be possible to achieve *at least* a count rate per 3°×3° channel of about 150 000 s^{-1} (the maximum that can be handled by current semiconductor detectors) and this yields ≈1.9 h/emission direction. With ≈450 emission directions in the symmetry-reduced $\frac{1}{8}$ of the hologram that would need to be covered for the case considered here, this yields a total time of 833 h=35 d. However, using multichannel semiconductor detection could reduce this by 5–20 times, if not more. The energy tunability of SR would also permit measuring interference patterns just above and just below the fluorescence threshold in question, and this should lead to more accurate methods of background subtraction. Due to the path-length-dependent phase factors present in the reconstruction algorithm, both XFH and EEH can in single-energy images and for high-symmetry geometries suffer from image cancellations due to the overlap of real and twin images when two scattering atoms are related by inversion symmetry. Using an experimental geometry of reduced symmetry or phased summations of reconstructions at different wave numbers will suppress these cancellation effects, although the latter procedure would not be possible for XFH.

This work was supported by the Department of Energy, Basic Energy Sciences, Materials Sciences Division, under Contract No. DOE-AC03-76SF00098, and the Office of Naval Research under Contract No. N00014-90-J-1457.

*Present address: Molecular Science Research Center, Pacific Northwest Laboratory, P.O. Box 999, MS K2-12, Richland, WA 99352.

†Also at Materials Science Division, Lawrence Berkeley Laboratory, Berkeley, CA 94720.

[1] A. Szöke, in *Short Wavelength Coherent Radiation: Generation and Applications*, edited by D. T. Attwood and J. Boker, AIP Conf. Proc. No. 147 (AIP, New York, 1986).

[2] (a) J. Barton, Phys. Rev. Lett. **61**, 1356 (1988); (b) **67**, 3106 (1991).

[3] D. K. Saldin *et al.*, Phys. Rev. B **44**, 2480 (1991); **45**, 9629 (1992), and references therein.

[4] S. Thevuthasan *et al.*, Phys. Rev. Lett. **70**, 595 (1993), and references therein.

[5] L. J. Terminello *et al.*, J. Vac. Sci. Technol. B **10**, 2088 (1992); Phys. Rev. Lett. **70**, 599 (1993), and references therein.

[6] C. S. Fadley, in *Synchrotron Radiation Research: Advances in Surface and Interface Science*, edited by R. Z. Bachrach (Plenum, New York, 1992); Surf. Sci. Rep. **19**, 231 (1993); in *Applications of Synchrotron Radiation Techniques to Materials Science*, edited by D. L. Perry *et al.*, MRS Symposia Proceedings No. 307 (Materials Research Society, Pittsburgh, 1993), p. 261.

[7] M. Tegze and G. Faigel, Europhys. Lett. **16**, 41 (1991).

[8] G. Materlik *et al.*, Phys. Rev. Lett. **52**, 441 (1984).

[9] J. T. Hutton *et al.*, Phys. Rev. B **31**, 743 (1985); **31**, 6420 (1985).

[10] (a) M. A. Van Hove and S. Y. Tong, *Surface Crystallography by LEED* (Springer-Verlag, New York, 1979); (b) B. W. Batterman and H. Cole, Rev. Mod. Phys. **36**, 681 (1964).

[11] *International Tables for X-ray Crystallography*, edited by K. Lonsdale (Reidel, Dordrecht, 1968), Vol. III.

[12] G. R. Harp *et al.*, Phys. Rev. Lett. **65**, 1012 (1990).

[13] D. K. Saldin and P. de Andres, Phys. Rev. Lett. **64**, 1270 (1990); K. Heinz *et al.*, Surf. Sci. Lett. **261**, 57 (1992).

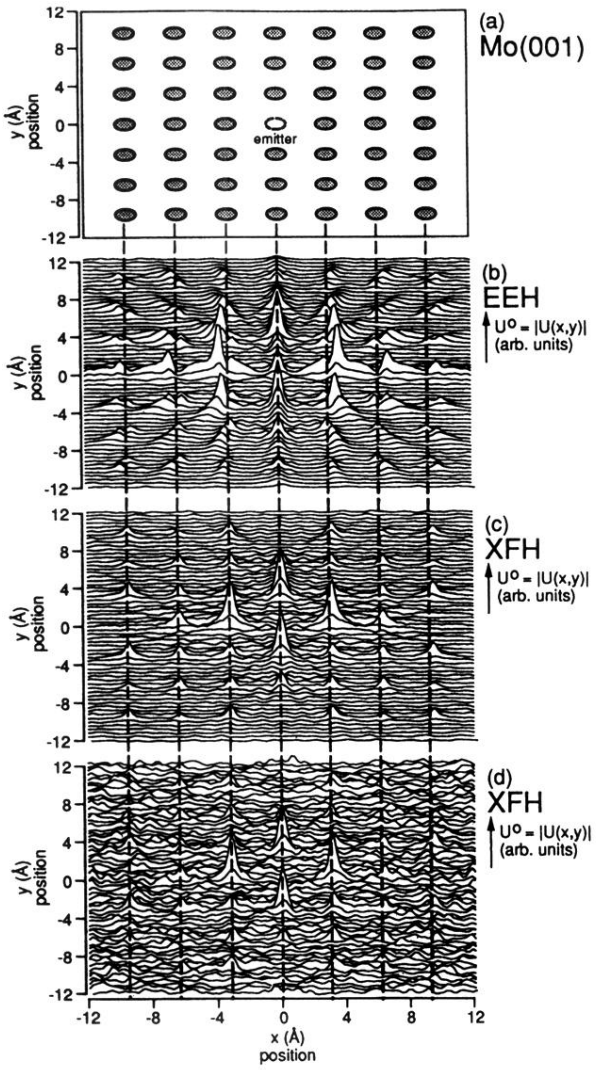

FIG. 1. (a) 49-atom Mo(001) cluster in the xy plane at $z = 0.0$ Å. (b) Image of the cluster in (a) as derived from the calculated electron-emission hologram (EEH) at 391 eV. (c) Image of the same cluster as derived from the calculated x-ray-fluorescence hologram (XFH) at 20.0 keV. Both electrons and x rays have a wavelength of 0.620 Å. (d) Image of the same cluster as derived from a simulated experimental XFH with statistical noise appropriate to 10^9 counts per direction.

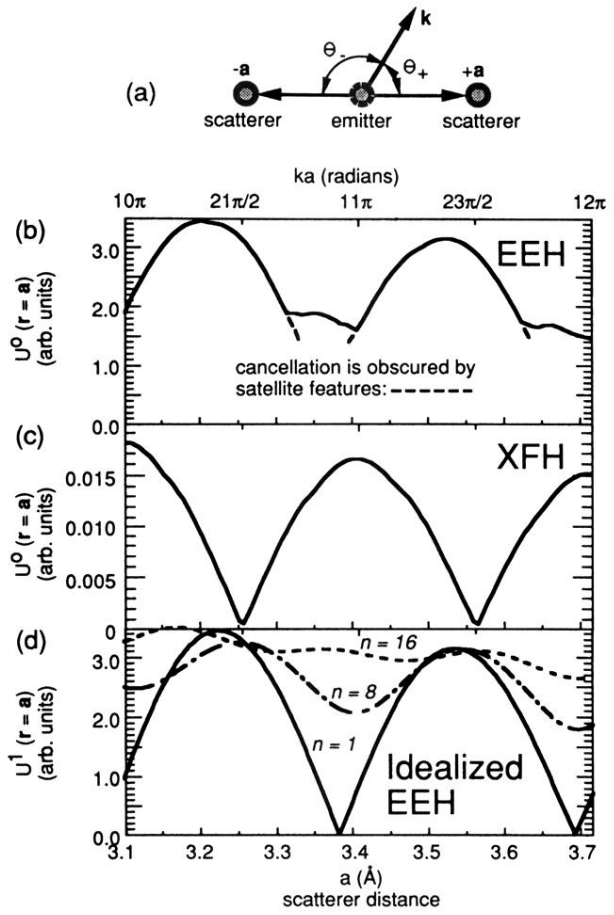

FIG. 3. (a) Three-atom Mo cluster, with a variable emitter-scatterer separation $|\mathbf{a}|$. Θ_+ is the scattering angle between $+\mathbf{a}$ and $\mathbf{k}$, and Θ_- is the scattering angle between $-\mathbf{a}$ and $\mathbf{k}$. Holographic reconstruction magnitudes $U^0(\mathbf{r}=\mathbf{a})$ and $U^1(\mathbf{r}=\mathbf{a})$ for the scatterer at $+\mathbf{a}$ as a function of $|\mathbf{a}|$ for (b) single-energy EEH; (c) single-energy XFH; (d) idealized phase-summed EEH using n different wave-number constructions.